

RESEARCH ARTICLE

# The P2X7 Receptor is a Master Regulator of Microparticle and Mitochondria Exchange in Mouse Microglia

Simonetta Falzoni<sup>1,†</sup>, Valentina Vultaggio-Poma<sup>1,†</sup>, Paola Chiozzi<sup>1</sup>, Mario Tarantini<sup>1</sup>, Elena Adinolfi<sup>1</sup>, Paola Boldrini<sup>2</sup>, Anna Lisa Giuliani<sup>1</sup>, Giampaolo Morciano<sup>1</sup>, Yong Tang<sup>3</sup>, Dariusz C. Gorecki <sup>4</sup>, Francesco Di Virgilio <sup>1,\*</sup>

<sup>1</sup>Department of Medical Sciences, University of Ferrara, 44100 Ferrara, Italy,, <sup>2</sup>Center for Electron Microscopy, University of Ferrara, 44100 Ferrara, Italy, <sup>3</sup>International Joint Research Centre on Purinergic Signalling & Chengdu University of Traditional Chinese Medicine, 610075 Chengdu, China and <sup>4</sup>School of Pharmacy and Biomedical Sciences, University of Portsmouth, P01 2DT Portsmouth, UK

\*Address correspondence to F.D.V. (e-mail: [fdv@unife.it](mailto:fdv@unife.it))

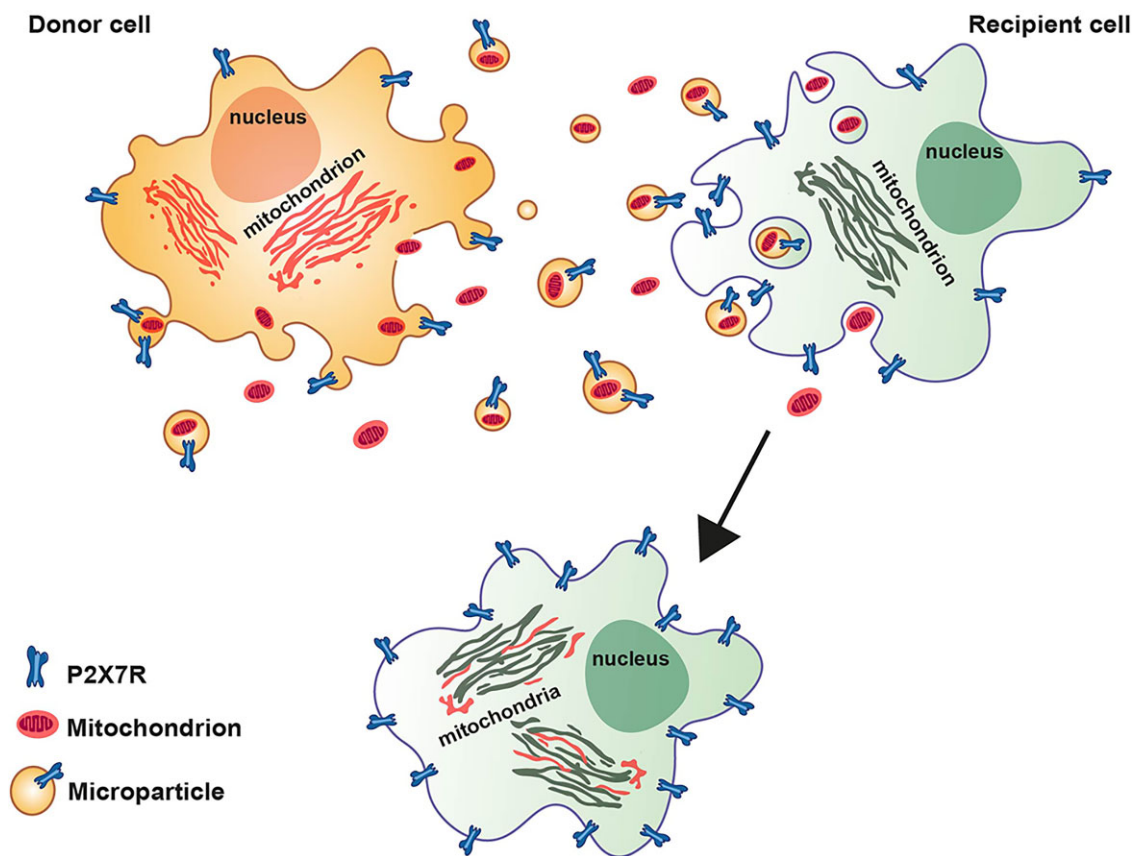
<sup>†</sup>Co-first Authorship

## Abstract

Microparticles (MPs) are secreted by all cells, where they play a key role in intercellular communication, differentiation, inflammation, and cell energy transfer. P2X7 receptor (P2X7R) activation by extracellular ATP (eATP) causes a large MP release and affects their contents in a cell-specific fashion. We investigated MP release and functional impact in microglial cells from P2X7R-WT or P2X7R-KO mice, as well as mouse microglial cell lines characterized for high (N13-P2X7R<sup>High</sup>) or low (N13-P2X7R<sup>Low</sup>) P2X7R expression. P2X7R stimulation promoted release of a mixed MP population enriched with naked mitochondria. Released mitochondria were taken up and incorporated into the mitochondrial network of the recipient cells in a P2X7R-dependent fashion. NLRP3 and the P2X7R itself were also delivered to the recipient cells. Microparticle transfer increased the energy level of the recipient cells and conferred a pro-inflammatory phenotype. These data show that the P2X7R is a master regulator of intercellular organelle and MP trafficking in immune cells.

Submitted: 20 February 2024; Revised: 10 April 2024; Accepted: 15 April 2024

© The Author(s) 2024. Published by Oxford University Press on behalf of American Physiological Society. This is an Open Access article distributed under the terms of the Creative Commons Attribution-NonCommercial License (<https://creativecommons.org/licenses/by-nc/4.0/>), which permits non-commercial re-use, distribution, and reproduction in any medium, provided the original work is properly cited. For commercial re-use, please contact [journals.permissions@oup.com](mailto:journals.permissions@oup.com)



**Key words:** P2X7 receptor; microparticles; mitochondria; microglia; inflammation

## Introduction

Information exchange is a vital function of all living organisms, whether unicellular or multicellular. Neurotransmitters, hormones, growth factors, and inflammatory mediators are usually released and travel across the intercellular space as individual molecules, but often they are packed in the lumen of exosomes/vesicles/particles, collectively referred to as microparticles (MPs), to be delivered to nearby or faraway target cells.<sup>1</sup> While exosomes originate from cytoplasmic multivesicular bodies, extracellular vesicles are the result of plasma membrane budding; thus, they usually contain cytoplasmic components, including mitochondria.<sup>2,3</sup> Mechanism of MP release has been the focus of intense scrutiny over the last two decades, leading to the identification of the crucial role played by extracellular ATP (eATP) acting at the P2X7 receptor (P2X7R).<sup>4-8</sup>

It is an established fact that eATP is an ubiquitous messenger accumulating at sites of trauma, cancer, or inflammation and also acting as a modulator of neurotransmission in the central nervous system (CNS).<sup>9,10</sup> Effects of eATP are mediated by the well-known P2 receptor family, notably at inflammatory and cancer sites by the P2X7R subtype.<sup>11</sup> Verderio and co-workers showed previously that astrocyte-derived eATP causes vesicle shedding from microglia.<sup>5</sup> We showed a similar effect of eATP in human dendritic cells.<sup>6,7</sup> The potent MP-releasing activity of eATP acting at the P2X7R has become textbook knowledge ever since.<sup>12</sup> This eATP effect is of special interest because, besides promoting MP release, this nucleotide also modulates MP contents and is itself carried by the MPs.<sup>8,13</sup> The discovery that MPs

contain functioning mitochondria that can be transferred to the target cells has added an additional level of interest and complexity to the pathophysiological function of these extracellular structures.<sup>2</sup>

Naked mitochondria have also been identified in the mixed vesicle population, collectively referred to as shed MPs.<sup>8,14</sup> We recently observed that a massive release of mitochondria-laden MPs as well as of naked functional mitochondria is triggered by eATP stimulation of mouse melanoma tumor cells via the P2X7R.<sup>8</sup> The function of extracellular free mitochondria is still debated; nonetheless, there is good evidence that these organelles undergo cell-to-cell transfer via tubular structures,<sup>15</sup> MP uptake,<sup>16</sup> or phagocytosis and can be incorporated into the target cell mitochondrial network. Mitochondria transfer is increasingly recognized as a key process in tissue repair,<sup>17</sup> in CNS homeostasis,<sup>18</sup> and in immune-cancer cell interaction, as a determinant of immune evasion.<sup>19</sup> While macrophages appear to be a leading participant in the process of mitochondrial transfer, both as donors and recipients,<sup>20</sup> much less is known about that role in microglia. In the CNS, there is good evidence that mitochondria transfer occurs between astrocytes and microglia, and bi-directionally between neurons and astrocytes,<sup>21</sup> but only scattered observations report an inter-microglia mitochondria transfer.<sup>22</sup> Exchange of mitochondria between neurons and glia, or between microglial cells, is thought to be relevant in a multiplicity of neuroinflammatory and neurodegenerative diseases, and thus potentially exploitable for therapeutic purposes.

In the present study, we set to investigate how P2X7R expression affects mitochondria release and microglia-to-microglia mitochondria transfer, and whether it modulates the MP cargo. To address this issue, we used primary microglia from P2X7R-WT or P2X7R-KO mice, as well as the N13 microglia cell line expressing high levels of the P2X7R (N13-P2X7R<sup>High</sup>), and a variant thereof selected in our laboratory for low P2X7R expression (N13-P2X7R<sup>Low</sup>). We found that P2X7R expression on the donor cells strongly affects both basal and eATP-stimulated MP release, as well as MP uptake by the target cells. The MP fraction released upon eATP stimulation contained a heterogeneous population of small vesicles, mitochondria-containing vesicles, and naked mitochondria. Upon interaction with the target cell, mitochondria and MP components (including the P2X7R itself) were transferred to the recipient cells. Microparticles derived from N13-P2X7R<sup>High</sup> very efficiently transferred the P2X7R to N13-P2X7R<sup>Low</sup>, thus enabling restoration of P2X7R-dependent responses, including reversible plasma membrane permeabilization, the hallmark of P2X7R function. Furthermore, the ability to generate multinucleated giant cells (MGCs), typical histological features of chronic inflammation, was also restored. Microparticle-mediated transfer between microglial cells might be an efficient mechanism for the modulation of neuroinflammation.

## Materials and Methods

### Experimental Model and Study Participant Details

#### Cell Culture

N13-P2X7R<sup>High</sup> and N13-P2X7R<sup>Low</sup> cells were grown in RPMI-1640 medium (Sigma–Aldrich, St. Louis, MO, USA) supplemented with 10% heat-inactivated FBS (Gibco, Thermo Fisher Scientific, Waltham, MA, USA), 100 U/mL penicillin, and 100 µg/mL streptomycin (both from Sigma–Aldrich, cat. # P4333) (complete medium). In some experiments, sucrose medium containing 300 mM sucrose, 1 mM K<sub>2</sub>HPO<sub>4</sub>, 1 mM MgSO<sub>4</sub>, 5.5 mM glucose, and 20 mM HEPES (pH 7.4) was used. Primary mouse microglial cells were isolated from 2-d-old C57BL/6 mice as described by Sanz et al.<sup>23</sup> and Lian et al.<sup>24</sup> Briefly, a mixed astrocyte/microglia population was seeded into cell culture flasks and incubated at 37°C in a CO<sub>2</sub> incubator for 5–7 d. To obtain microglia, the flasks were shaken, and the floating cells collected. Microglial cells were plated in high glucose DMEM supplemented with 2 mM GlutaMAX<sup>TM</sup> (Gibco, Thermo Fisher Scientific), 10% heat-inactivated FBS, 100 U/mL penicillin, and 100 µg/mL streptomycin (complete medium). Animal experimentation was carried out under authorization from the Italian Ministry of Health (n. 744/2018-PR and n. 264/2021-PR).

### Method Details

#### Microparticle Preparation

N13-P2X7R<sup>High</sup> and N13-P2X7R<sup>Low</sup> cells ( $5 \times 10^5$  cells) were seeded into 6-well plates in complete medium and cultured overnight. Cells were then rinsed and further maintained in fresh complete medium in presence or absence of 0.4 mM ATP for 24 h in a CO<sub>2</sub> incubator at 37°C. Primary mixed glial cells were cultured in T75 cm<sup>2</sup> tissue culture flask in complete medium for 9–12 d. Cells were then rinsed and further maintained in complete medium (without serum) in presence or absence of 0.2 mM Bz-ATP for 12 h in a CO<sub>2</sub> incubator at 37°C.

Then, the cell supernatant was withdrawn and centrifuged at  $800 \times g$  for 10 min to remove floating cells and cell debris.

Microparticles were then isolated by centrifugation at  $10\,000 \times g$  for 1 h at 4°C.

#### Staining With CellTrace<sup>TM</sup> Carboxyfluorescein Succinimidyl Ester, Calcein/AM, MitoTracker Green, or MitoTracker Red

Cells ( $5 \times 10^5$ ) or MPs thereof were incubated in complete RPMI medium in the presence of CellTrace<sup>TM</sup> carboxyfluorescein succinimidyl ester (CFSE) (5 µM) (Thermo Fisher Scientific, cat. # C34554), calcein/AM (1 µg/mL) (Thermo Fisher Scientific, cat. # C1430), MitoTracker Green FM (400 nm) (Thermo Fisher Scientific, cat. # M7514), or MitoTracker Red FM (400 nm) (Thermo Fisher Scientific, cat. # M22425) in a CO<sub>2</sub> incubator for 20 min at 37°C. At the end of this incubation cells were rinsed and resuspended in fresh complete RPMI medium, while MPs were washed with warm (37°C) PBS, centrifuged at  $10\,000 \times g$  for 30 min, and resuspended in 500 µL of either complete RPMI or sucrose medium. Fluorescence was analyzed in a thermostat-controlled (37°C) and magnetically stirred Cary Eclipse fluorescence spectrophotometer (Agilent Technologies, Milano, Italy) or with a confocal microscope (LSM Carl Zeiss, Oberkochen, Germany) equipped with a plan-apochromat 63x oil immersion objective. Living primary microglial cell images were acquired with a confocal laser scanning microscope Olympus FV3000, equipped with a 60x oil immersion lens (numerical aperture 1.4), a digital zoom of 2x, and a pinhole set at 1 airy unit on thermostated (37°C) and humidity-controlled (CO<sub>2</sub> 5%) stage. 488 nm and 561 nm excitation lasers were used to acquire Mitotracker green and Mitotracker red probes, respectively.

#### Oxygen Consumption

Oxygen consumption was measured according to the recommended protocol, “O<sub>2</sub> kit Abcam” (cat. # AB197243). Briefly, the MP pellet isolated from  $5 \times 10^5$  cells was suspended in 100 µL of sucrose solution supplemented with 0.2 mM CaCl<sub>2</sub>, and transferred to a fluorimeter cuvette containing 400 µL of sucrose solution supplemented with 1 mM EGTA to a final volume of 500 µL. This MP suspension was then incubated with 40 µL of Abcam reagent. Oxygen consumption was measured at the 340 and 642 nm excitation and emission wavelengths, respectively, in the thermostat-controlled fluorescence spectrophotometer (Agilent Technologies) described above for 30 min. Carbonyl cyanide-p-trifluoromethoxyphenylhydrazone (FCCP) (2.5 µM), or oligomycin (10 µg/mL) were added as a stimulant or an inhibitor, respectively, of mitochondrial respiration.

#### Cell Proliferation Assay

Cell proliferation assay was performed using the crystal violet technique. Briefly,  $10^4$  cells per well were plated in 12-well plate and cultured at 37°C in a CO<sub>2</sub> incubator in the presence or absence of MPs isolated from either N13-P2X7R<sup>High</sup> or N13-P2X7R<sup>Low</sup> cells stimulated with 0.4 mM eATP. At the 0, 24, 48, and 72 h time points cells were fixed with 4% paraformaldehyde, stained with 0.1% crystal violet, extracted with acetic acid 10%, and analyzed by spectrophotometry (OD 595 nm) in a microplate reader (Wallac Victor3 1420, PerkinElmer, Wellesley, MA, USA).

#### Measurement of Microparticle and Cellular ATP Content

ATP was measured in MP or cell lysates with the luciferase/luciferin method (Enliten luciferase/luciferin cat. # FF2021, Promega, Italy) in a Firezyme luminometer (Biomedica Diagnostics Inc, Windsor, Canada). Data were expressed as relative luminescence units (RLU) and converted into ATP concentration with an appropriate calibration curve.

### Measurement of Microparticle Potential

Microparticle membrane potential ( $\Delta\psi_m$ ) was qualitatively measured by monitoring the uptake of the positively charged tetramethylrhodamine methyl ester (TMRM) (Thermo Fisher Scientific, cat. # I34361) at a concentration of 10 nM by confocal microscopy at an emission wavelength of 570 nm, as previously described.<sup>25</sup>

### Western Blotting

Cells and MPs were lysed in the following lysis buffer: 300 mM sucrose, 1 mM  $K_2HPO_4$ , 1 mM  $MgSO_4$ , 5.5 mM glucose, 20 mM HEPES, 1 mM benzamidine, 1 mM phenylmethylsulfonyl fluoride (PMSF), 0.2  $\mu$ g/mL DNase (cat. # D5025), and 0.3  $\mu$ g/mL RNase (cat. # R5875) (all Sigma-Aldrich). Proteins were separated on NuPage Bis-Tris 4%-12% precast gel (Thermo Fisher Scientific cat. # NP0335BOX) and transferred to nitrocellulose membrane (GVS Life Sciences cat. # I228243). After incubation for 1 h with TBS-Tween-20 (0.1%) (Sigma-Aldrich, cat. # P9416) supplemented with 2.5% non-fat powdered milk and 0.5% BSA to saturate unspecific binding sites, membranes were incubated overnight with primary antibodies at 4°C. The anti-NLRP3 polyclonal antibody (Novus, cat. # NBP2-12446) was diluted 1:500. The anti-cytochrome C rabbit antibody (cat. # Ab 133504, Abcam), anti-VDAC/porin rabbit polyclonal antibody (cat. # Ab 15895, Abcam), anti-TOM20 rabbit polyclonal antibody (Merck, cat. # HPA011562), anti-TIM23 rabbit polyclonal antibody (Thermo Fisher Scientific, cat. # PA5-71877), anti-P2X7R polyclonal antibody (Merck, cat. # P8232), and anti-carbonic anhydrase II polyclonal antibody (Merck, cat. # HPA001550) were used at the 1:1000 dilution. Membranes were incubated with a secondary goat anti-rabbit HRP-conjugated antibody (Thermo Fisher Scientific, cat. # A16096) at 1:3000 dilutions for 1 h at room temperature.

### Transmission Electron Microscopy (TEM) of Isolated Microparticles

The MP pellet obtained as described was fixed with 1% paraformaldehyde and 1.25% glutaraldehyde in 0.15 M cacodylate buffer, postfixed in 2% osmium tetroxide, dehydrated by sequential passages in increasing acetone concentrations, and included in Araldite Durcupan ACM (Merck, cat. # 44613). Ultrathin sections were prepared with the Reichert Ultracut S ultramicrotome, counterstained with uranyl acetate in saturated solution and lead citrate according to Reynolds,<sup>26</sup> and analyzed with Hitachi H800 (Hitachi High Technologies Corporation, Brughiero, Italy), or Thermo Fisher Scientific™ Talos™ L120C transmission electron microscopes (TEM).

### Immunogold Labeling of Isolated Microparticles

Microparticles were fixed in 0.4% paraformaldehyde and permeabilized with 0.05% Triton X-100 at room temperature in PBS for 20 min, followed by incubation at room temperature in 2% BSA-supplemented PBS for 20 min to block nonspecific binding. Microparticles were then incubated overnight with the primary anti-TOM20 rabbit polyclonal antibody (Merck, cat. # HPA011562) diluted 1:100 in 0.2% BSA-containing PBS. Microparticles were thoroughly washed in PBS and bound antibodies were detected with protein A coated with 20-nm gold at the final dilution of 1:100 in 0.2% BSA-containing PBS. Finally, MPs were rinsed in PBS and processed for electron microscopy.

### Lucifer Yellow Uptake

N13-P2X7R<sup>High</sup> or N13-P2X7R<sup>Low</sup> were seeded in 24-well plastic dishes (20 × 10<sup>4</sup> per well) in complete RPMI medium for 24 h. Cells were then rinsed and incubated in 300  $\mu$ L of a saline solution containing 125 mM NaCl, 5 mM KCl, 1 mM  $MgSO_4$ , 1 mM

$NaH_2PO_4$ , 20 mM HEPES, 5.5 mM glucose, 250  $\mu$ M sulfinpyrazone, 5 mM  $NaHCO_3$ , and 1 mM  $CaCl_2$ , pH 7.4, supplemented with 1 mg/mL lucifer yellow. ATP was then added at the concentration of 3 mM and the monolayers were incubated in a CO<sub>2</sub> incubator (37°C). After 15 min, 5 mM  $MgSO_4$  was added to each well to chelate excess ATP<sup>4-</sup>, the monolayers were rinsed twice with the above saline solution and further incubated in 400  $\mu$ L of FBS- and phenol red-free RPMI for microscopy. To quantitate lucifer yellow fluorescence, cells were lysed with 4  $\mu$ L of Triton X-100 for 10 min under continuous stirring, supernatants were withdrawn, and fluorescence quantitated fluorimetrically at the excitation/emission wavelength pair 428/540. Fluorescence was normalized on the protein content measured by the Bradford method.

### Real Time PCR

Total RNA was extracted from cells or MPs with Trizol Reagent (Thermo Fisher Scientific, cat. # 1559626), and purified with the Pure Link RNA kit (Thermo Fisher Scientific, cat. # 12183018A) as per the manufacturer's instructions. One  $\mu$ g of total mRNA was reverse transcribed with the High Capacity cDNA Reverse Transcription Kit (Thermo Fisher Scientific, cat. # 4374966). Two microliter of cDNA were used as a template for qRT-PCR. TaqMan probes for expression of P2X7R (Thermo Fisher Scientific, cat. # Mm00440578.m1) and NOD-LRR- and pyrin domain-containing protein 3 (NLRP3) (Thermo Fisher Scientific, cat. # Mm00840904.m1) genes and TaqMan probe for G3PDH housekeeping gene were selected from the ready-to-use gene expression assay (Thermo Fisher Scientific, cat. # 435239E). A comparative analysis using the  $\Delta\Delta$ CT method was used to quantitate the fold increase of target cDNA relative to N13 cells.

### Statistical Analysis

Data were analyzed with the GraphPad Prism 9 software (GraphPad Software, Inc., La Jolla, CA, USA). Statistical significance was calculated with either a two-tailed Student's t or ANOVA test, assuming equal SD and variance. All data are shown as the mean  $\pm$  standard error of the mean (SEM). Differences were considered significant at  $P < 0.05$ . Coding: \* $P < 0.05$ ; \*\* $P < 0.01$ ; \*\*\* $P < 0.001$ ; \*\*\*\* $P < 0.0001$ .

## Results

Resting or stimulated microglial cells are known to release a mixed population of MPs of different sizes containing both exosomes and plasma membrane-derived extracellular vesicles.<sup>5,12</sup> Accumulating evidence supports a key role of the P2X7R in MP release in microglia as well as in other cell types.<sup>6,7,27,28</sup> N13-P2X7R<sup>High</sup> and N13-P2X7R<sup>Low</sup> microglial cells were loaded with the cytoplasmic marker dyes calcein/AM (Figure 1A-D) or CFSE (Figure 1E-H), then rinsed and incubated in the absence or presence of either eATP or the more potent analogue benzoyl-ATP (Bz-ATP). As shown in Figure 1, N13-P2X7R<sup>High</sup> cells (Figure 1A and B), but not N13-P2X7R<sup>Low</sup> (Figure 1C and D), released MPs into the culture medium within a few minutes of incubation in the presence of the P2X7R agonists. Challenge with eATP (Figure 1E) or Bz-ATP (Figure 1F), up to a concentration of 1 or 0.5 mM, respectively, significantly increased MP release from N13-P2X7R<sup>High</sup> cells, several fold and time-dependently (Figure 1H), while MP release from N13-P2X7R<sup>Low</sup> was negligible. Microparticle release was linearly related to the eATP but not to the Bz-ATP concentration, arguably because BzATP concentrations higher than 0.3 mM cause necrotic cell death. Both eATP- and Bz-ATP-stimulated MP release was mitigated, albeit not fully inhibited, by pretreatment

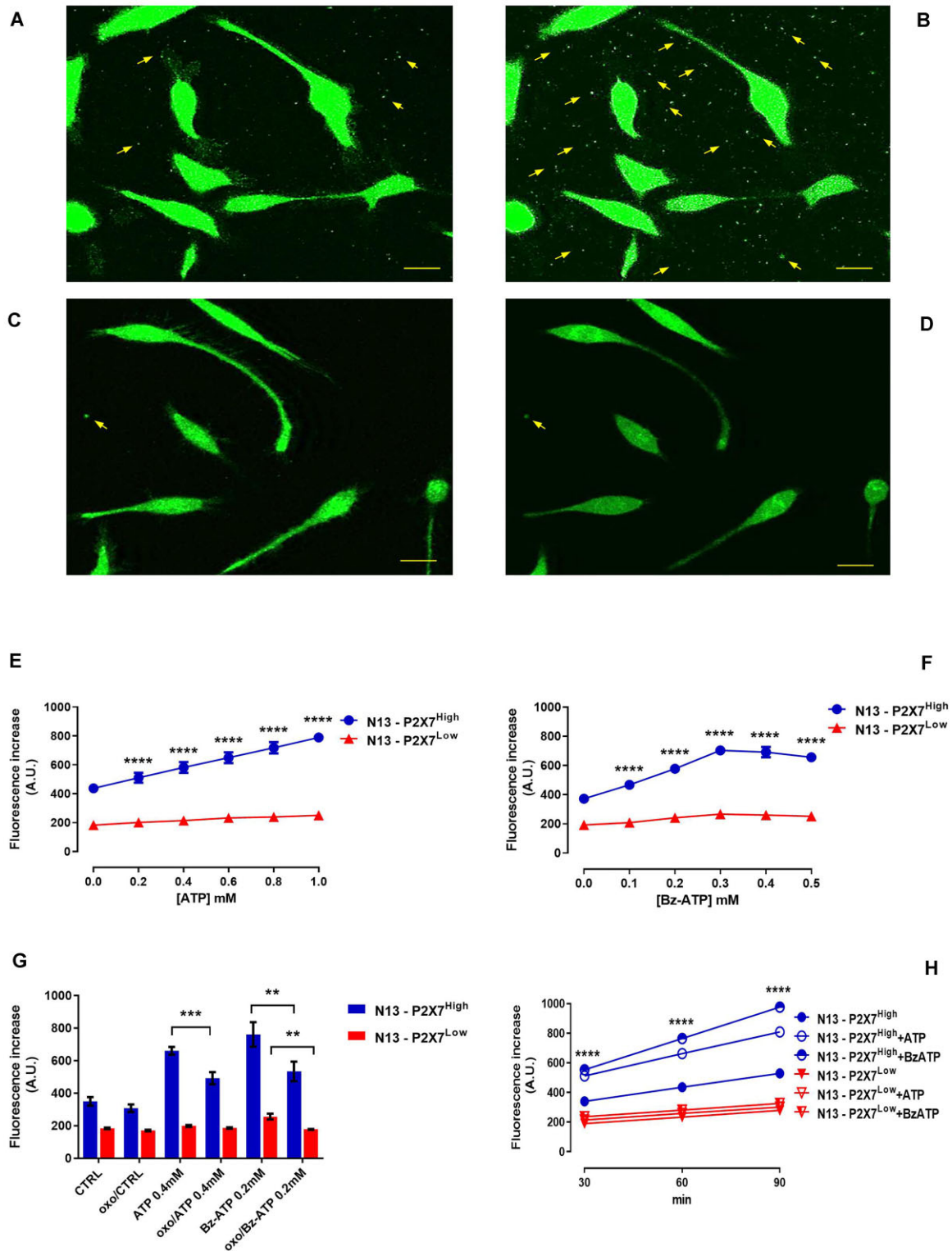


**Figure 1.** N13 microglial cells release MPs in a P2X7R-dependent fashion. Five  $\times 10^5$  N13-P2X7R<sup>High</sup> (A) or N13-P2X7R<sup>Low</sup> (C) cells were loaded with the cytoplasmic marker calcein/AM (1  $\mu$ g/mL) in RPMI complete culture medium for 20 min, then rinsed, re-suspended in the same medium, and challenged with 0.4 mM eATP for 15 min to trigger MP (arrow) release [B, eATP-stimulated N13-P2X7R<sup>High</sup>; D, eATP-stimulated N13-P2X7R<sup>Low</sup>]. (E-H) Cells were loaded with CFSE (5  $\mu$ M) and incubated with increasing concentrations of eATP (E) or BzATP (F) for 60 min. (G) Cells were treated with 0.3 mM oxidized ATP (oxo) for 1 h at 37 $^{\circ}$ C prior to stimulation with either eATP or BzATP. (H) Time course of MP release in the presence or absence of either 0.4 mM eATP or 0.2 mM BzATP. To measure MP fluorescence, cell supernatants were withdrawn, centrifuged at 10 000  $\times g$  (4 $^{\circ}$ C) for 1 h to concentrate the MPs, and the pellet re-suspended in 500  $\mu$ L of sucrose medium. Fluorescence was measured in a fluorimeter cuvette at the 488/520 nm wavelength pair. Data are means  $\pm$  SEM of three to four experiments each performed in triplicate. \*\* =  $P < 0.01$ ; \*\*\* =  $P < 0.001$ ; \*\*\*\* =  $P < 0.0001$  by Student t-test (E-G), or two-way ANOVA (H). Fluorescence images were acquired with a Nikon Eclipse TE 300 inverted fluorescence microscope equipped with a 40 $\times$  objective and fluorescein filters. Bar = 10  $\mu$ m.

with the potent covalent P2X7R blocker oxidized-ATP (oxo-ATP) (Figure 1G), as previously shown.<sup>29</sup> P2X7R blockade did not fully prevent MP release due to the likely stimulation of P2Y receptors by ATP as well as BzATP.<sup>30</sup>

N13-P2X7R<sup>High</sup> cells were then labeled with the selective mitochondrial marker Mitotracker Green FM and left unchallenged (Figure 2A) or stimulated with eATP (Figure 2B). Besides intracellular organelles, also extracellular MPs were stained by this dye, suggesting that they contain mitochondria (Figure 2A and B, arrows). To further characterize the mitochondrial content, MPs were isolated, as described in Materials and Methods, from the supernatants of resting (Figure 2C and D), or eATP-stimulated (Figure 2E and F) N13-P2X7R<sup>High</sup> microglia, incubated in the presence of either calcein/AM (Figure 2C and E) or the selective, potential-sensitive mitochondrial stain Mitotracker Red FM (Figure 2D and F), and analyzed for fluorescence emission. Henceforth, MPs released from N13-P2X7R<sup>High</sup> or N13-P2X7R<sup>Low</sup> microglia will be referred to as MP-P2X7R<sup>High</sup> or MP-P2X7R<sup>Low</sup>, respectively. As shown in Figure 2G, calcein-positive MPs are about twice as many as those positive for Mitotracker Red, suggesting that either not all calcein-positive MPs contain mitochondria, or that calcein- and MitoTracker Red-positive extracellular vesicles are separate MP populations. To verify this latter hypothesis, we co-labeled the source N13-P2X7R<sup>High</sup> cells with both calcein/AM and MitoTracker Red FM prior to eATP challenge. Image merging showed that quite a few MPs were yellow, indicating co-localization, and suggested that the MP fraction contained a mixed population of naked mitochondria, MPs containing mitochondria, and mitochondria-less MPs (Figure 2H).

To further verify the presence of mitochondria, MPs were examined by transmission electron microscopy (TEM) and labeled with immunogold using an antibody against a specific transporter of the outer mitochondrial membrane (TOM20). Microparticle-P2X7R<sup>High</sup>, recovered from the supernatant of eATP-stimulated N13-P2X7R<sup>High</sup> cells, contained naked mitochondria (Figure 2I) that were specifically labeled by the anti-TOM20 antibody (Figure 2J). Thus, as previously shown by us and by other investigators,<sup>2,8,31</sup> MPs are a rather heterogeneous population containing a plethora of intracellular molecules and even intracellular organelles, including mitochondria. Microparticles, whether released spontaneously (Figure 2K) or upon eATP stimulation (Figure 2L-N), were also strongly stained by the potential-sensitive dye TMRM, a further proof of a membrane potential, negative inside. Accordingly, addition of the mitochondrial uncoupler FCCP (Figure 2M) or of the electron transport chain inhibitor rotenone (Figure 2N) fully abrogated TMRM fluorescence.

As additional characterization, we probed by Western blotting the MP fraction for canonical mitochondrial markers, for the inflammasome protein NLRP3, and for the P2X7R itself. Microparticle-P2X7R<sup>Low</sup> compared to MP-P2X7R<sup>High</sup> had a lower content of Cyt C, VDAC1, TOM20, and TIM23, as well as of NLRP3 and P2X7R (Figure 3A-H). Challenge of the N13-P2X7R<sup>High</sup> or N13-P2X7R<sup>Low</sup> cells with eATP or BzATP caused a marked increase in the content of mitochondrial markers, P2X7R and NLRP3 in MP-P2X7R<sup>High</sup>, but a significantly lower one in MP-P2X7R<sup>Low</sup>.

A highly heterogeneous MP population containing vesicles of various sizes and mitochondria was also released by primary microglia (Supplementary Figure S1). Interestingly, MPs released from P2X7R-KO microglia contained less material compared to those from P2X7R-WT, and mitochondria were distinctly smaller, as previously shown by our laboratory.<sup>32</sup> Stimulation with BzATP (or with ATP) also increased the MP content of P2X7R

and of the mitochondrial markers TIM23 and TOM20 (Supplementary Figure S2). An increase in the MP content of these markers was also caused by BzATP stimulation of P2X7R-KO microglia, suggesting that also other P2 receptors, likely P2Y receptors, contribute to BzATP-stimulated mitochondria release.<sup>30</sup>

Besides NLRP3 and P2X7R proteins, MPs also contained their respective mRNAs (Figure 3I and J). Challenge of N13-P2X7R<sup>High</sup> with eATP had a differential effect on the NLRP3 and P2X7R mRNA content in both the source cells and in the released MP-P2X7R<sup>High</sup>, as NLRP3 mRNA was increased while P2X7R mRNA was decreased (Figure 3I and J). Again, changes in NLRP3 or P2X7R mRNA levels in the eATP-stimulated MP-P2X7R<sup>Low</sup> were negligible.

Despite the identification of mitochondria in the MP fraction by morphological, biochemical, and immunolabeling techniques and demonstration of a FCCP-sensitive membrane potential, the formal proof that mitochondria in the MP fraction were able to support respiration and associated oxidative phosphorylation (OxPhos) was still required. Thus, we investigated whether MPs support O<sub>2</sub> consumption sensitive to canonical mitochondrial poisons such as FCCP and oligomycin. We were unable to use the SeaHorse technology since it was impossible to make MP adhere to the bottom of SeaHorse dishes without damaging the MPs themselves; thus, we turned to a fluorometric technique based on O<sub>2</sub> quenching of the Abcam reagent (see Materials and Methods). Microparticles exhibited a basal oxygen consumption that was further stimulated by FCCP and fully blocked by oligomycin, thus confirming its dependency on ATP synthesis (Figure 3K). In agreement with the higher mitochondrial content, unstimulated MP-P2X7R<sup>High</sup> accumulated an about 10-fold higher iATP content compared to MP-P2X7R<sup>Low</sup> (Figure 3L). The iATP content of MP-P2X7R<sup>High</sup>, and to a lesser extent that of MP-P2X7R<sup>Low</sup>, was further enhanced by stimulation with eATP or Bz-ATP of the respective source cells prior to the MP collection (Figure 3L).

We next investigated the fate of the released MPs to verify whether, as reported in other cell types, they might be taken up by target microglial cells. Donor N13-P2X7R<sup>High</sup> or N13-P2X7R<sup>Low</sup> cells ( $5 \times 10^5$ ) were labeled with Mitotracker Green FM. Then, MPs released over a 24-h incubation were recovered as described in Materials and Methods, and the same dose of MPs administered either to unlabeled N13-P2X7R<sup>High</sup> or to unlabeled N13-P2X7R<sup>Low</sup> “target” cells. Unlabeled N13-P2X7R<sup>High</sup> cells were incubated for 24 h with Mitotracker Green FM-labeled MP-P2X7R<sup>High</sup>, rinsed, and then analyzed (Figure 4A). This prolonged co-incubation caused a strong staining of intracellular vesicular and filamentous structures in the recipient unlabeled N13-P2X7R<sup>High</sup>. Alternatively, unlabeled N13-P2X7R<sup>Low</sup> cells were incubated with Mitotracker Green-labeled MP-P2X7R<sup>High</sup>. In this case, staining of intracellular structures was much weaker. Then, unlabeled N13-P2X7R<sup>High</sup> cells were challenged with Mitotracker Green-labeled MP-P2X7R<sup>Low</sup>, and finally, N13-P2X7R<sup>Low</sup> were challenged with Mitotracker Green-labeled MP-P2X7R<sup>Low</sup>. In both these latter cases, staining of intracellular organelles in the recipient cells was very weak, albeit slightly stronger when N13-P2X7R<sup>High</sup> were challenged with MP-P2X7R<sup>Low</sup>.

To verify that mitochondria in the MP fraction transferred to the target cells were able to fuse with the endogenous mitochondrial network, recipient N13-P2X7R<sup>High</sup> (Figure 4B, upper panels) or N13-P2X7R<sup>Low</sup> cells (Figure 4B, lower panels) were labeled with Mitotracker Red FM, and co-incubated in the presence of Mitotracker Green FM-labeled MP-P2X7R<sup>High</sup>. Within 6 h, nearly all the added MPs were taken up by N13-P2X7R<sup>High</sup> but not by N13-P2X7R<sup>Low</sup>. Image merging showed an almost perfect colocalization with the endogenous, red-stained

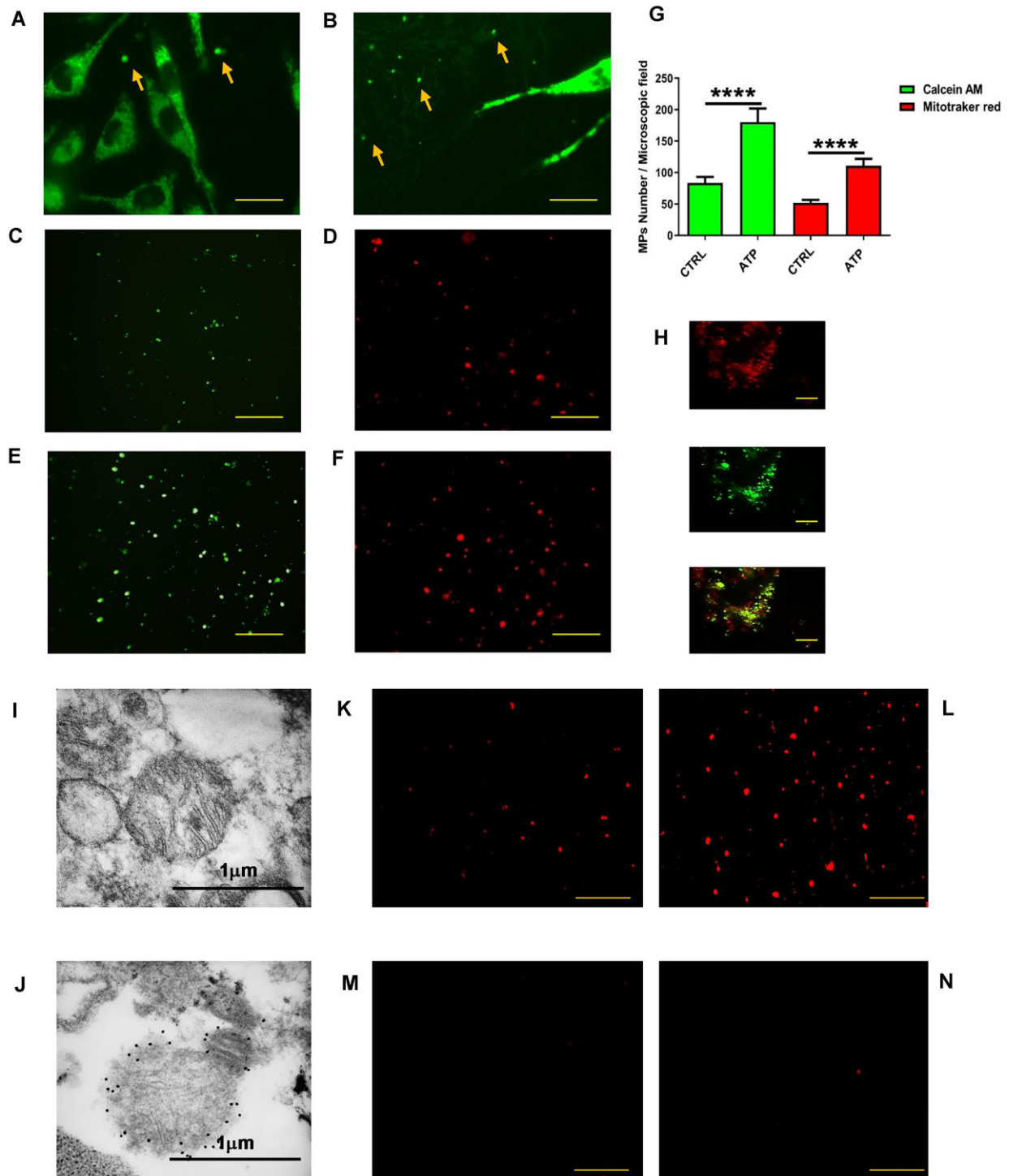


**Figure 2.** Released MPs contain mitochondria. N13-P2X7R<sup>High</sup> (A, B) cells ( $10^5$ ) were seeded onto 13-mm-diameter round glass coverslip and stained with the mitochondrial selective dye MitoTracker Green FM (200 nM) for 15 min at 37°C. The coverslips were then placed on the heated (37°C) stage of a Nikon inverted microscope as described in the legend to Figure 1, and either left unchallenged (A) or stimulated with 0.4 mM eATP for 5 min (B). Yellow arrows indicate MitoTracker Green FM-stained MPs. In panels C-F, supernatants from resting (C, D) or 0.4 mM eATP-stimulated (E, F) N13-P2X7R<sup>High</sup> were stained with calcein/AM (C, E) or MitoTracker Red FM (D, F) and analyzed with a Zeiss LSM510 confocal microscope equipped with a 63× oil immersion plan-apochromat objective. (G) Calcein/AM- or MitoTracker Red FM-positive MPs released from resting or eATP-stimulated N13-P2X7R<sup>High</sup> cells released over a 60-min timespan were quantitated. (H) Microparticles released over a 24 h incubation period from eATP (0.4 mM)-challenged N13-P2X7R<sup>High</sup> cells co-labeled MitoTracker Red FM (200 nM) and calcein/AM (1 μM), were isolated as described in Materials and Methods and analyzed by confocal microscopy with rodhamine (upper) or fluorescein (middle) filters, and merged (lower). Microparticles isolated from N13-P2X7R<sup>High</sup> were analyzed by TEM without (I) or with (J) immunogold labeling with an antibody against the specific mitochondrial protein TOM20. Microparticles isolated from resting (K) or 0.4 mM eATP-stimulated (L-N) N13-P2X7R<sup>High</sup> were stained with TMRM and analyzed by confocal microscopy. 2.5 μM FCCP (M), or 200 nM rotenone (N) were also added. Bars = 20 μm (A-F), 10 μm (H, K-N). Data are means ± SEM from three independent experiments each performed in triplicate. \*\*\*\* P < 0.0001 by unpaired t test.

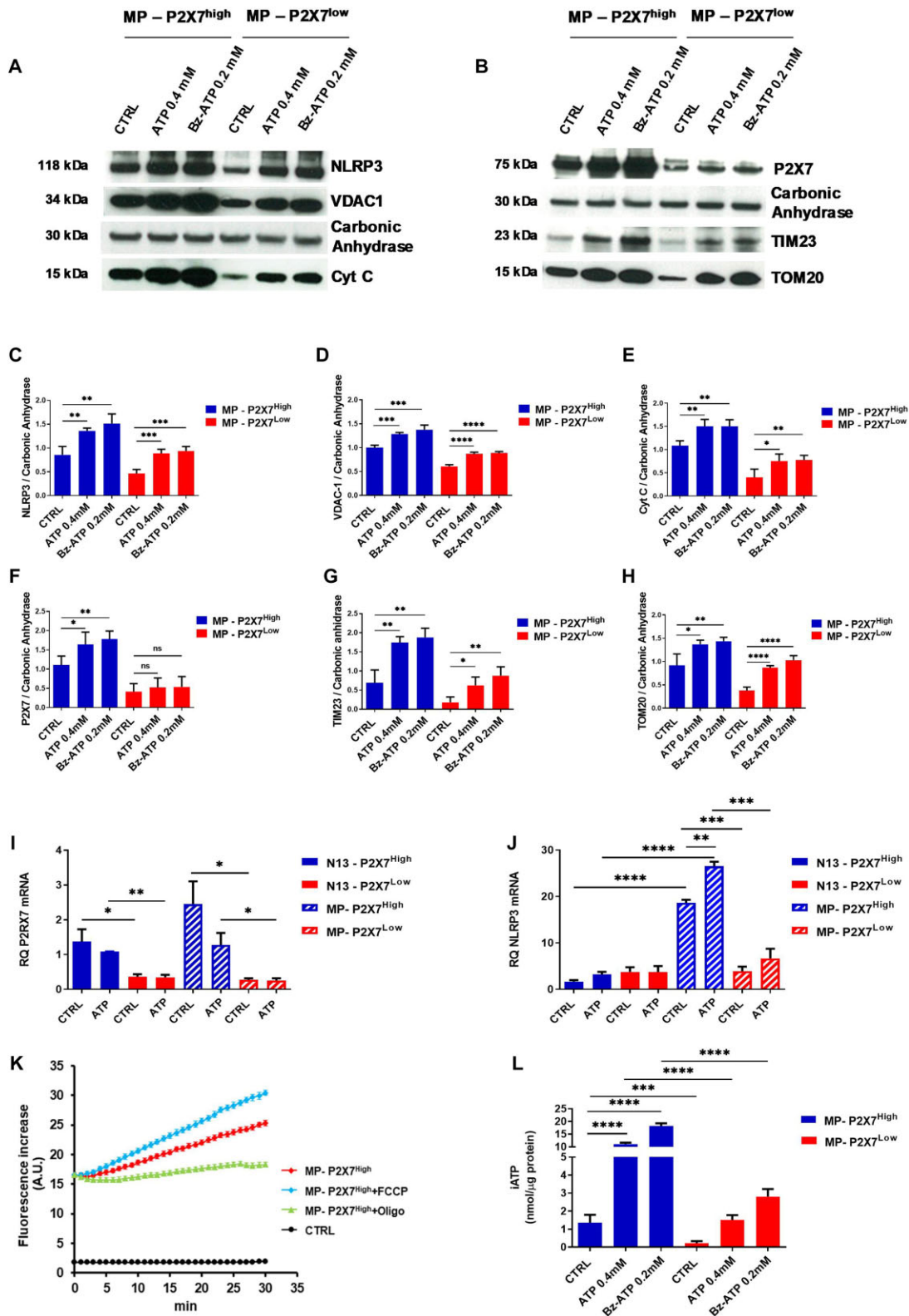


**Figure 3.** Microparticle-P2X7<sup>High</sup> compared to MP-P2X7<sup>Low</sup> express higher levels of NLRP3, P2X7 and mitochondrial markers. N13-P2X7<sup>High</sup> and N13-P2X7<sup>Low</sup> cells were plated in 75 cm<sup>2</sup> culture flasks and stimulated with 0.4 mM eATP or 0.2 mM BzATP for 24 h. At the end of this incubation, MPs were isolated and processed for Western Blotting analysis (A, B) as described in Materials and Methods. Carbonic anhydrase was used as a loading control. Densitometry (C-H) was performed with ImageJ software. mRNA was isolated from control or eATP-stimulated (0.4 mM) MPs (P2X7R, I), (NLRP3, J), and from MPs released during a 24-h incubation. CTRL: control resting cells. (K) Oxygen consumption by MP-P2X7<sup>High</sup> in the absence or presence of FCCP or oligomycin. Control (CTRL): O<sub>2</sub> consumption in the absence of MPs. (L) Intracellular ATP (iATP) content of MP-P2X7<sup>High</sup> and MP-P2X7<sup>Low</sup>. ATP was measured as described in Materials and Methods. Data are means ± SEM from three to four independent experiments. \* P < 0.05; \*\* P < 0.01; \*\*\* P < 0.001; \*\*\*\* P < 0.0001 by unpaired t test.

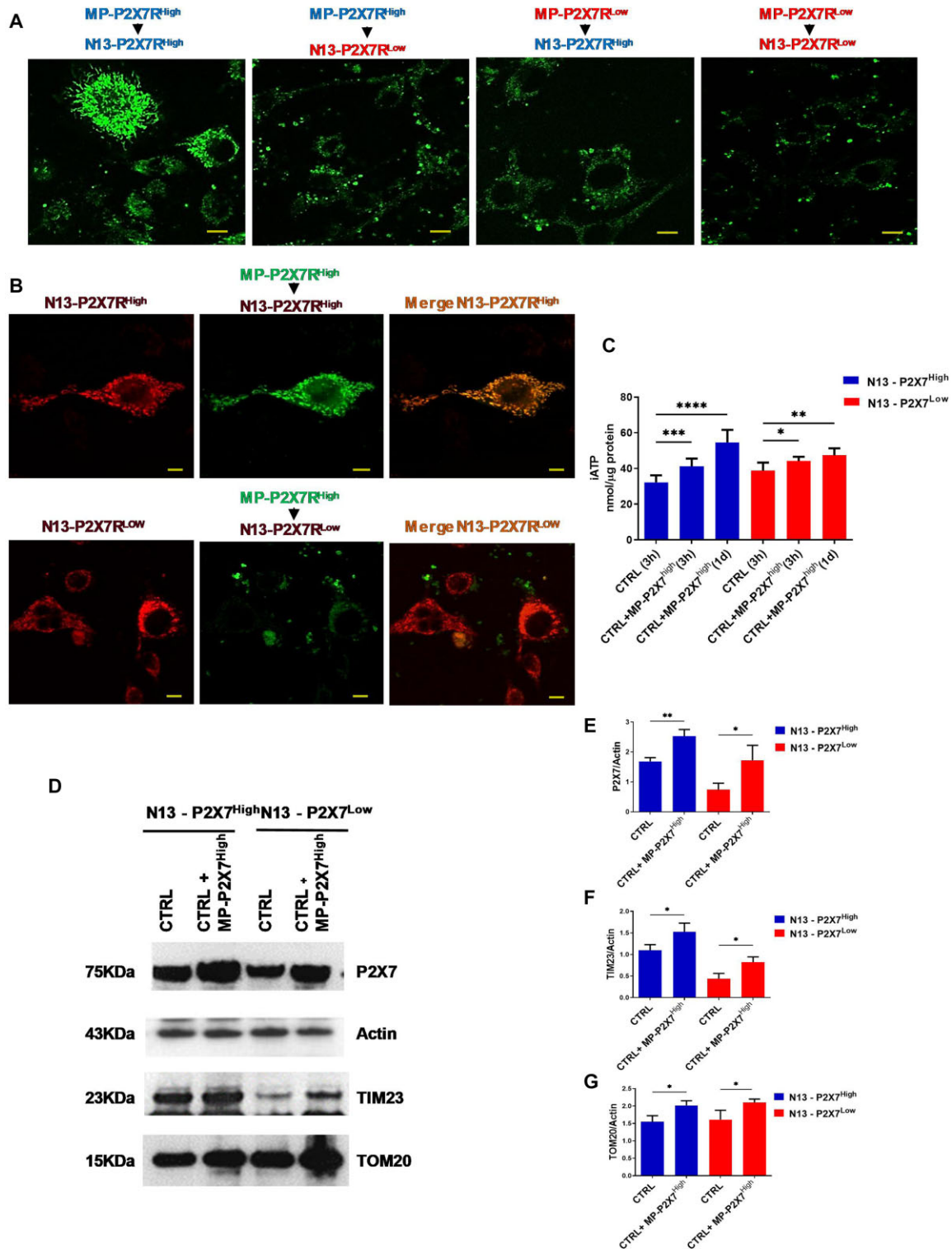


**Figure 4.** Released mitochondria are taken up by target N13 microglial cells in a P2X7R-dependent fashion. (A) Unlabeled N13-P2X7R<sup>High</sup> or N13-P2X7R<sup>Low</sup> were let adhere to 24-well dishes, rinsed, and further incubated in complete RPMI medium for 24 h with MitoTracker Green FM-labeled MP-P2X7R<sup>High</sup> or MP-P2X7R<sup>Low</sup> previously isolated from MitoTracker Green FM-labeled source N13 cells (see Materials and Methods). At the end of this incubation, the monolayers were rinsed to remove extracellular MPs, fresh medium was added, and the cells analyzed by confocal microscopy as described in the legend to Figure 1. (B) N13-P2X7R<sup>High</sup> (upper panel) or N13-P2X7R<sup>Low</sup> (lower panel) were loaded with MitoTracker Red FM (400 nm) at 37°C for 20 min, then thoroughly rinsed and further incubated at 37°C in complete RPMI medium for 24 h with MP-P2X7R<sup>High</sup> released from MitoTracker Green-stained N13-P2X7R<sup>High</sup>. At the end of this incubation period cells were analyzed by confocal microscopy. (C) Intracellular ATP content of N13-P2X7R<sup>High</sup> or N13-P2X7R<sup>Low</sup> after 3 or 24 h (1 d) of co-incubation with MP-P2X7R<sup>High</sup>. (D) WB of control or MP-P2X7R<sup>High</sup>-pulsed N13-P2X7R<sup>High</sup> or N13-P2X7R<sup>Low</sup> cell lysates. Actin was used as loading control. (E-G) Densitometric analysis. Isolation of MP-P2X7R<sup>High</sup> and co-incubation with either N13-P2X7R<sup>High</sup> or N13-P2X7R<sup>Low</sup> were performed as described in Materials and Methods. (A) Bar = 20 μm; B, bar = 10 μm. \* P < 0.05; \*\* P < 0.01; \*\*\* P < 0.001; \*\*\*\* P < 0.0001 by unpaired t test.

mitochondrial network in N13-P2X7R<sup>High</sup> but far less in N13-P2X7R<sup>Low</sup> cells (merge). Mitochondria uptake also enhanced the total ATP content of the recipient cells, but especially of the N13-P2X7R<sup>High</sup>, since iATP levels in these cells after a 24 h (1 d) incubation in the presence of MPs almost doubled (Figure 4C). Furthermore, co-incubation of N13-P2X7R<sup>High</sup> or N13-P2X7R<sup>Low</sup> with MP-P2X7R<sup>High</sup> increased the TIM23, TOM20, and P2X7R content of the recipient cells (Figure 4D-G).

Transfer of mitochondria also occurred in primary microglia. Recipient cells from P2X7R-WT mice were challenged with MPs isolated from N13P2X7<sup>High</sup> cells (Figure 5A), and after 6 h examined for MP uptake. Image merging showed a substantial co-localization, suggesting fusion of the supplemented mitochondria with the endogenous mitochondrial network. Then, MP-N13P2X7<sup>Low</sup> were administered to microglia from P2X7R-WT mice, but in this case little uptake occurred, and merging showed almost no colocalization (Figure 5B). Microglia from P2X7-KO mice showed very little MP uptake and no colocalization, whether challenged with MP-P2X7R<sup>High</sup> or MP-P2X7R<sup>Low</sup> (Figure 5C-D). We were forced to use in these experiments MPs originating from the N13 cell line rather than from primary microglia because the amount of MPs released from primary cells was too small to allow visualization of a reproducible uptake.

To rule out the possibility that spillover of green or red fluorescence might at least partially confuse the mitochondria uptake and colocalization analysis, we run control experiments with single fluorochrome-labeled cells showing that there was absolutely no spillover of red fluorescence into the green channel and vice versa (Supplementary Figure S3).

Next, we verified whether MPs challenge could modify cell responses. Cells with high P2X7R expression exhibit the peculiar reversible permeabilization of the plasma membrane triggered by exposure to eATP,<sup>33-35</sup> a feature witnessed by lucifer yellow uptake by N13-P2X7R<sup>High</sup> cells (Figure 6A). In contrast, N13-P2X7R<sup>Low</sup> microglia was refractory to eATP-mediated permeabilization, as shown by near-absent dye uptake (Figure 6C). Incubation in the presence of MP-P2X7R<sup>High</sup> only slightly enhanced the already high lucifer yellow uptake in N13-P2X7R<sup>High</sup> cells (Figure 6B) but had a significant impact on this dye uptake in N13-P2X7R<sup>Low</sup> cells (Figure 6D). Measurement of cell-associated fluorescence shows that incubation in the presence of MP-P2X7R<sup>High</sup> almost doubled lucifer yellow uptake by N13-P2X7R<sup>Low</sup> cells (Figure 6E). In addition, incubation of N13-P2X7R<sup>High</sup> cells in the presence of MP-P2X7R<sup>High</sup> almost doubled their proliferation rate, both at the 48 and 72 h time points (Figure 6F). The effect of the incubation of N13-P2X7R<sup>High</sup> with MP-P2X7R<sup>Low</sup> was much smaller, albeit still statistically significant (Figure 6F). N13-P2X7R<sup>Low</sup> cells showed a lower basal proliferation rate compared to N13-P2X7R<sup>High</sup>, a well-known feature of P2X7R-less cells,<sup>36-38</sup> and their proliferation was enhanced by incubation with MP-P2X7R<sup>High</sup> and to a lesser extent with MP-P2X7R<sup>Low</sup> (Figure 6G).

Expression of the P2X7R confers several inflammatory features to mononuclear phagocytes, among which is the ability to generate MGCs,<sup>39</sup> typical of chronic granulomatous inflammation. We previously showed that P2X7R-less phagocytes are unable to undergo spontaneous fusion,<sup>39,40</sup> thus we investigated whether fusion of N13 microglia was enhanced after incubation with MPs isolated from either N13-P2X7R<sup>Low</sup> or N13-P2X7R<sup>High</sup>. Multinucleated giant cell formation was measured in N13-P2X7R<sup>High</sup> cultures incubated for 48 h alone (Figure 7A), in the presence of MP-P2X7R<sup>Low</sup> (Figure 7B), or MP-P2X7R<sup>High</sup> (Figure 7C). As shown quantitatively in Figure 6D, fusion increased over

time to finally decline after 48 h, as previously documented,<sup>39</sup> likely due to the accelerated necrosis of the MGCs. Fusion was accelerated significantly by co-incubation with MP-P2X7R<sup>High</sup> but not with MP-P2X7R<sup>Low</sup> (Figure 7D); however, co-incubation in the presence of MP-P2X7R<sup>High</sup> also accelerated MGC necrosis (Figure 7C). Contrary to N13-P2X7R<sup>High</sup>, N13-P2X7R<sup>Low</sup> cells were unable to generate MGCs spontaneously (Figure 7E); however, their fusion was greatly enhanced by the presence of MP-P2X7R<sup>High</sup> (Figure 7G), but not MP-P2X7R<sup>Low</sup> (Figure 7F). The strong potentiation of MGC formation promoted by co-incubation in the presence of MP-P2X7R<sup>High</sup> was quantitated in Figure 7H.

## Discussion

We show here that the P2X7R is a master regulator of exchange of functioning mitochondria and MP by microglia. Intercellular transfer of mitochondria via different routes (tunneling nanotubes, MPs, connexins, and uptake of secreted naked mitochondria) is a novel means of information transfer active in most tissues, including epithelia, neuronal cells, immune cells, and cancer cells.<sup>41</sup> This mechanism appears to fulfill different needs, such as disposal of damaged mitochondria but also refurbishment of stressed cells with healthy mitochondria. This may have important pathophysiological implications, as the supply of cancer cells with functioning mitochondria has been shown to enhance tumor ability to escape immune surveillance.<sup>19</sup> Furthermore, the transfer of potent damage-associated molecular patterns (DAMPs) such as mitochondrial DNA and cytochrome C is inherently prone to ignite or amplify inflammation.

In the brain, an organ eminently susceptible to mitochondrial dysfunction and thus heavily affected by mitochondrial pathologies, mitochondrial transfer might have a very important pathophysiological role. Likewise, mitochondria are implicated in neuroinflammation.<sup>42</sup> Accumulating evidence shows that astrocytes transfer mitochondria to neurons,<sup>17</sup> and vice versa that damaged mitochondria are transferred from neurons to astrocytes.<sup>18</sup> Microglia is also able to exchange mitochondria with astrocytes<sup>43</sup> or with other microglial cells.<sup>22</sup> The rationale for such exchange activity seems to be, on the one hand, the acceleration of dysfunctional mitochondria disposal and, on the other, the propagation of pro-inflammatory signals. Of relevance, results by Watson et al.<sup>44</sup> suggest that microglia are highly effective in the *in vitro* and *in vivo* transfer of mitochondria to glioblastoma tumors, thus increasing tumorigenicity. This is in line with the observations by Sengupta and co-workers showing the potent cancer-promoting effect of mitochondria transfer from immune to cancer cells.<sup>19</sup>

Macrophages are heavily involved in the transcellular mitochondria exchange, both as donor and recipient cells. This has been shown to occur in the adipose tissue, lungs, heart, and likely in the bone marrow via several mechanisms, i.e., phagocytosis, tunneling nanotubes, or extracellular vesicle uptake.<sup>20</sup> Although intercellular mitochondria transfer also occurs in the CNS, the mechanism of mitochondria release and uptake by microglia has been little investigated.

Mitochondria transfer is a powerful mean for the modulation of inflammation. Uptake of stem cell-derived mitochondria by macrophages promotes M2 polarization and downmodulates inflammation.<sup>45</sup> Furthermore, in the adipose tissue under physiological conditions an intense intercellular mitochondria trafficking occurs between adipocytes and macrophages.<sup>46</sup> Paradoxically, the main product of mitochondrial metabolic activity, i.e.,

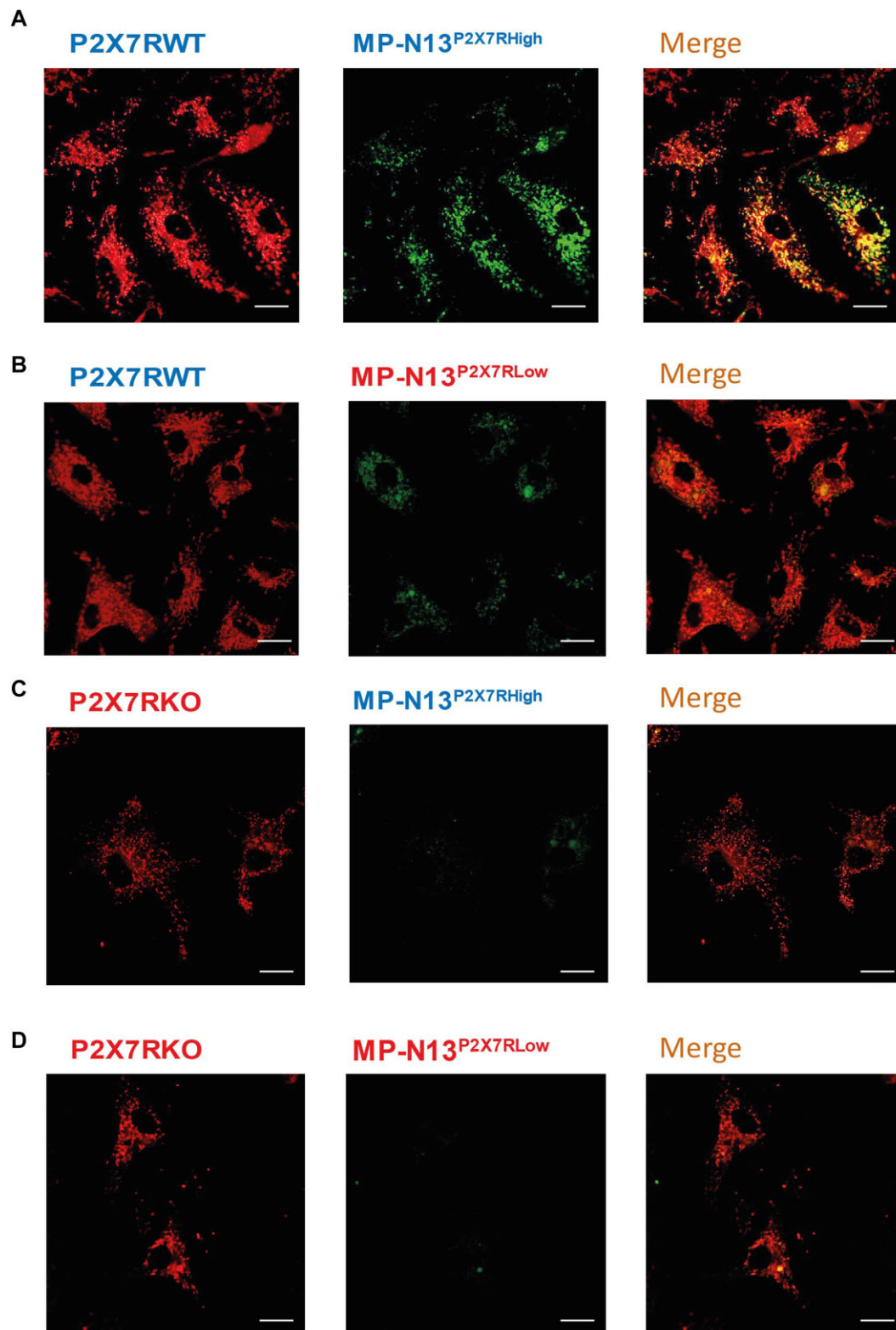


**Figure 5.** Released mitochondria are taken up by primary microglia in a P2X7R-dependent fashion. Mitotracker Red-labelled microglial cells from P2X7R-WT or P2X7R-KO mice were let adhere to 24-well dishes, rinsed, and further incubated in complete RPMI medium for 24 h with MitoTracker Green FM-labeled MP-P2X7R<sup>High</sup> or MP-P2X7R<sup>Low</sup> previously isolated from MitoTracker Green FM-labeled source N13 cells (Materials and Methods). At the end of this incubation, the monolayers were rinsed to remove extracellular MPs, fresh medium was added, and the cells analyzed by confocal microscopy as described in the legend to [Figure 1](#). Bars = 5  $\mu$ m.

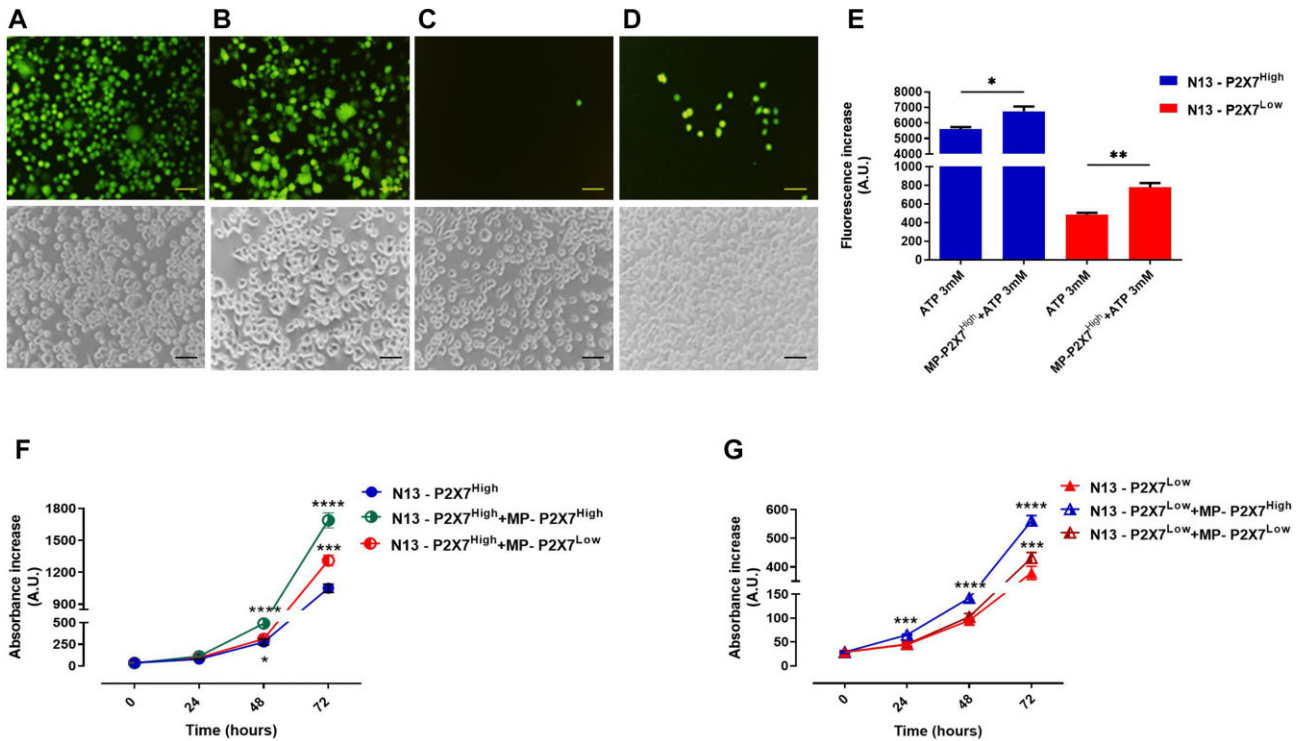


**Figure 6.** Fusion of MP-P2X7R<sup>High</sup> with the recipient cells restores eATP-mediated plasma membrane permeabilization and increases the proliferation rate in a P2X7R-dependent fashion. Fluorescence (A-D, upper panels) or phase contrast (A-D, lower panels) images of eATP-stimulated lucifer yellow uptake of control (A) or MP-P2X7R<sup>High</sup>-challenged (B) N13-P2X7R<sup>High</sup>, or control (C) or MP-P2X7R<sup>High</sup>-challenged (D) N13-P2X7R<sup>Low</sup>. Cells were incubated in complete RPMI medium at 37°C in a CO<sub>2</sub> incubator in the absence or presence of MP-P2X7R<sup>High</sup> for 24 h, then rinsed, further incubated in complete RPMI at 37°C, and challenged with 3 mM eATP in the presence of 1 mg/mL lucifer yellow. At the end of this incubation, the monolayers were thoroughly rinsed, incubated in fresh complete RPMI medium and analyzed by fluorescence microscopy with a IMT-2 Olympus phase/fluorescence microscope equipped with 20× objective. (E) Lucifer yellow fluorescence was quantitated as described in Materials and Methods. N13-P2X7R<sup>High</sup> (F) or N13-P2X7R<sup>Low</sup> (G) were seeded at 37°C in a CO<sub>2</sub> incubator in 24-well plastic dishes in complete RPMI medium. After an overnight incubation, a suspension of either MP-P2X7R<sup>High</sup> or MP-P2X7R<sup>Low</sup> was added to each given cell type, and incubation carried out at 37°C in a CO<sub>2</sub> incubator for further 72 h. Cell number was quantitated by crystal violet (see Materials and Methods). Bars = 50 μm. \* *P* < 0.05; \*\* *P* < 0.01; \*\*\* *P* < 0.001; \*\*\*\* *P* < 0.0001 by unpaired *t* test.

ATP, is also a powerful and omnipresent inflammatory mediator<sup>47,48</sup> and a most potent stimulant of extracellular vesicle (or MP) release from brain microglia.<sup>5</sup> This seems to be an integrated pro-inflammatory system, as eATP acting at P2X7R, a plasma membrane receptor highly expressed by mononuclear phagocytes, microglia included, promotes MP release.<sup>35, 49</sup>

The low MP release from N13-P2X7R<sup>Low</sup> reported in the present study confirms that in microglia P2X7R expression is a strong, albeit not absolute, requirement for MP release stimulated by eATP, or by its more potent agonist Bz-ATP. In fact, P2Y receptors are also likely to participate in this process. This conclusion is supported by the incomplete inhibition of MP shedding by the poorly selective P2X7R antagonist oxoATP shown in this study, or by the highly selective anti-P2X7R monoclonal antibody L4 previously reported by us.<sup>6</sup> The MP population is highly heterogeneous, including small (about 100-200 nm) and large (100-1000 nm) MPs as well as naked mitochondria. Expression of the P2X7R on the donor cell heavily affects the MP mitochondria content, as MP-P2X7R<sup>Low</sup> showed a much lower level of all specific mitochondrial markers compared to MP-P2X7R<sup>High</sup> and accordingly had a lower content of ATP. The reason for the reduced mitochondria content in MP-P2X7R<sup>Low</sup> might be twofold: on the one hand, N13-P2X7R<sup>Low</sup> have a lower mitochondrial metabolism<sup>32</sup> and content compared to N13-P2X7R<sup>High</sup>, on the other mitochondria trapping within the budding MPs or mitochondria extrusion might be less efficient in N13-P2X7R<sup>Low</sup> microglia. It has been proposed that the dispatch via MPs might

be a mean to dispose of malfunctioning mitochondria. However, our data show that MP-associated mitochondria are mostly functional. In fact, functionality is a key feature of the transferred mitochondria since their uptake and incorporation in the endogenous mitochondrial network improved the energy metabolism in recipient cells. Indeed, a 24-h incubation of N13-P2X7R<sup>High</sup> microglia in the presence of MP-P2X7R<sup>High</sup> caused a near doubling of the iATP content in the recipient cells, thus proving that supply of healthy mitochondria increases energy levels in these cells.

The MP cargo includes many bioactive molecules besides intracellular organelles, e.g., NLRP3 and P2X7R proteins as well as their respective mRNAs, thus suggesting that the MP uptake may increase the overall pro-inflammatory activity of the recipient cells. This is clearly shown by the conferment of P2X7R-dependent responses to N13-P2X7R<sup>Low</sup> cells, possibly due to the direct transfer of P2X7R, which is then directly incorporated into the plasma membrane. Another possibility is the translation of the MP-delivered mRNA. Co-incubation with MP-P2X7R<sup>High</sup> increased P2X7R protein levels in N13-P2X7R<sup>Low</sup> cells and made them susceptible to eATP-mediated reversible plasma membrane permeabilization, the hallmark of P2X7R activity. Additional functional responses of recipient cells, such as proliferation, were drastically affected by coincubation with MP-P2X7R<sup>High</sup>. The two-fold increase in proliferation might be due to the increased cell energetics as well as to enhanced P2X7R expression. Supply of functioning (“healthy”) mitochondria was

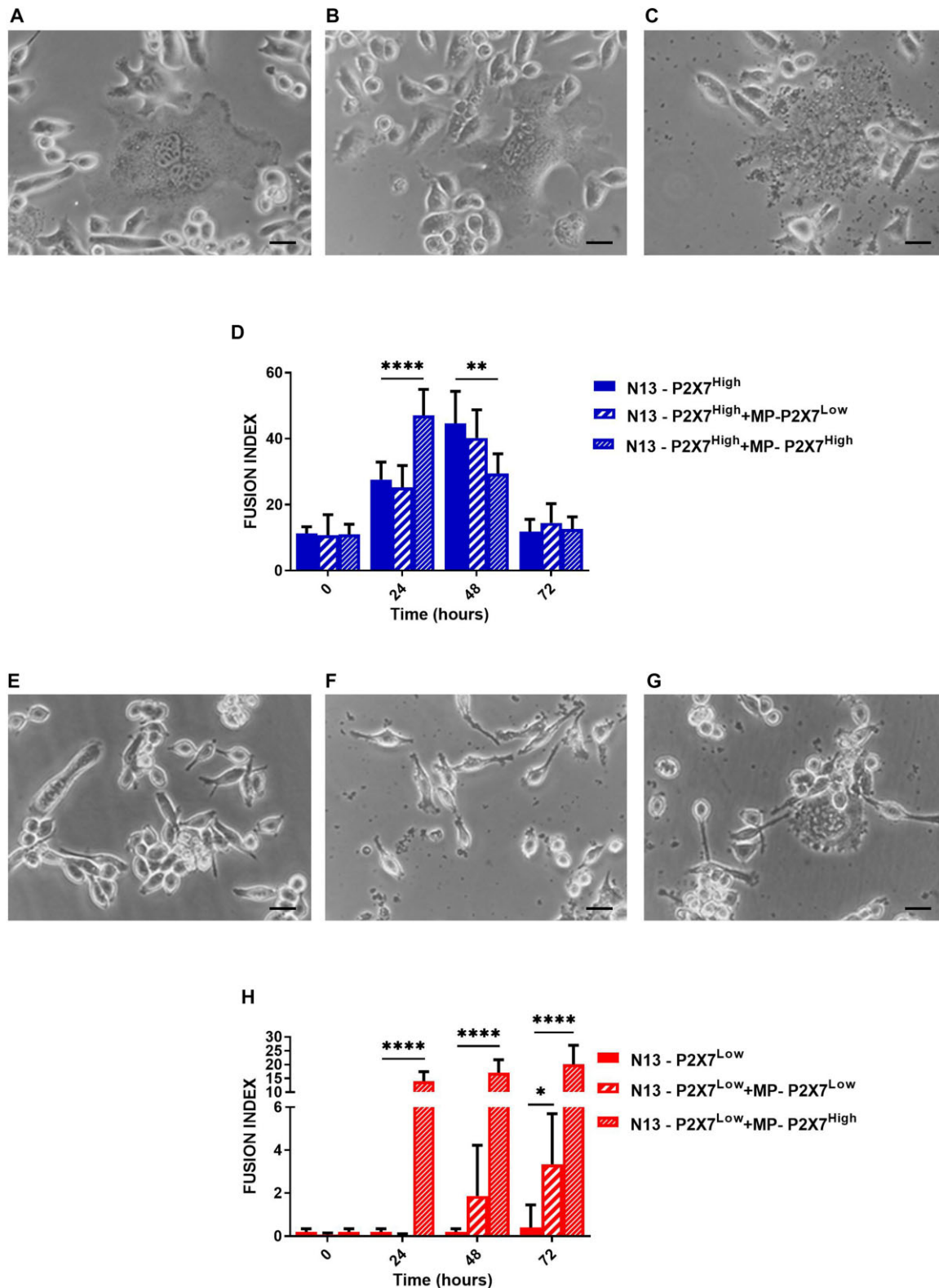


**Figure 7.** Microparticle fusion with the recipient cells enhances MGC formation in a P2X7R-dependent fashion. N13-P2X7<sup>High</sup> were incubated in 24-well plastic dishes at 37°C in complete RPMI medium for 48 h as such (A) or in the presence of either MP-P2X7<sup>Low</sup> (B) or MP-P2X7<sup>High</sup> (C). Time course of MGC formation shown as fusion index in N13-P2X7<sup>High</sup> monolayers incubated in the presence of MP-P2X7<sup>Low</sup>, MP-P2X7<sup>High</sup>, or left unchallenged (D). N13-P2X7<sup>Low</sup> were incubated in 24-well plastic dishes at 37°C in complete RPMI medium for 48 h as such (E) or in the presence of either MP-P2X7<sup>Low</sup> (F) or MP-P2X7<sup>High</sup> (G). Time course of MGC formation in N13-P2X7<sup>Low</sup> monolayers incubated in the presence of MP-P2X7<sup>Low</sup>, MP-P2X7<sup>High</sup>, or left unchallenged (H). Fusion index was calculated as follows: (number of nuclei within MGC/total number of nuclei) × 100. All pictures were taken with an Olympus microscope, as described in the legend to Figure 6. Bars = 10 μm. \*\* P < 0.01; \*\*\* P < 0.001; \*\*\*\* P < 0.0001 by unpaired t test.

shown to potentiate some key macrophage functions such as M2 polarization and phagocytosis,<sup>45,50</sup> likely to occur due to the increased iATP content. Also, increased P2X7R expression due to MP delivery might concur in the stimulation of cell growth, since basal activation of this receptor has trophic/growth-promoting effect.<sup>36</sup>

Among the most striking albeit often neglected properties of mononuclear phagocytes, microglia included, is their ability to undergo extensive cell fusion to generate MGCs, a hallmark of chronic granulomatous inflammation.<sup>39</sup> Ability to undergo spontaneous fusion in the absence of stimulation with inflammatory cytokines is fully dependent on P2X7R expression.<sup>39,51</sup> Incubation with MP-P2X7R<sup>High</sup> enhanced fusion in N13-P2X7R<sup>High</sup> cultures and more interestingly, conferred this ability to N13-P2X7R<sup>Low</sup> that are normally unable to fuse. This is yet another demonstration of the efficient MP-mediated transfer of bioactive molecules, and of their ability to promote a range of inflammatory responses.

To achieve optimal transfer of the MP cargo, expression of P2X7R on the plasma membrane of both the recipient and donor cells is needed. This might be due to the well-documented fusogenic effect of the P2X7R present on the membranes of both interactors,<sup>39</sup> or possibly due to a higher phagocytic activity of P2X7R-expressing cells. Furthermore, the P2X7R is known to promote phagocytosis and enhance pinocytosis in microglia,<sup>52,53</sup> thus increasing uptake of the MP cargo.

In conclusion, these data show that the P2X7R is a key determinant of MP trafficking in mouse microglia being needed both on the donor and recipient cells. P2X7R-expressing MPs efficiently transfer their mitochondrial cargo to the target cells, thus enhancing their energetics and modulating their key functionalities. Given the role of eATP and P2X7R in inflammation, these findings help to better understand the complex modulation of microglia functions in neuroinflammation and neurodegeneration.

## Author Contributions

S.F., V. V.-P., G.M. and P.C. performed most of the experiments and data analysis; M.T. analyzed part of the data and revised the study; E.A. and A.L.G. help design the study and revised the text; P.B. was responsible for TEM; Y.T. reviewed the MS, and D.G. and F.D.V. designed the study and wrote the paper.

## Supplementary Material

Supplementary material is available at the APS Function online.

## Funding

The work described in this study was supported by grants from the Italian Association for Cancer Research (n. IG 18581, IG 22883 and IG 22837) to FDV and EA, the Ministry of Education of Italy (PRIN n. 20178YTNWC), the Cure Alzheimer Fund (USA), the Royal Society Exchange Fellowship IES\R3\170196, PUR-THER Transcan-3 Project STC 2021, the PNRR Project “Mnesys” funded by the European Community, and institutional funds from the University of Ferrara. This publication is based upon work from PRESTO COST Action CA21130 supported by COST (European Cooperation in Science and Technology).

## Conflict of Interest

FDV is a member of the Scientific Advisory Board of Biosceptre Ltd (Australia), a biotech Company involved in the development of anti-P2X7 antibodies, and a Consultant with Breye Therapeutics ApS (Denmark). The other authors declare no conflict of interest. FDV is an inventor and owner of the following patent:

(1) Chimeric proteins for measuring ATP concentrations in the pericellular space and related screening method. 2005. European Patent Office number RM2005A000252-SG/IC.

FDV, SF, and MT are inventors and owners of the following patent:

(2) Ratiometric probe for the measurement of the extracellular ATP concentration. 2023. Filed, allowance pending.

## Data Availability

The data underlying this article will be shared on reasonable request to the corresponding author

## References

- van Niel G, D'Angelo G, Raposo G. Shedding light on the cell biology of extracellular vesicles. *Nat Rev Mol Cell Biol*. 2018;**19**(4):213–228.
- Hough KP, Trevor JL, Strenkowski JG, et al. Exosomal transfer of mitochondria from airway myeloid-derived regulatory cells to T cells. *Redox Biol* 2018;**18**: 54–64.
- D'Souza A, Burch A, Dave KM, et al. Microvesicles transfer mitochondria and increase mitochondrial function in brain endothelial cells. *J Control Release* 2021;**338**: 505–526.
- MacKenzie A, Wilson HL, Kiss-Toth E, Dower SK, North RA, Surprenant A. Rapid secretion of interleukin-1beta by microvesicle shedding. *Immunity* 2001;**15**(5):825–835.
- Bianco F, Pravettoni E, Colombo A, et al. Astrocyte-derived ATP induces vesicle shedding and IL-1 beta release from microglia. *J Immunol* 2005;**174**(11):7268–7277.
- Pizzirani C, Ferrari D, Chiozzi P, et al. Stimulation of P2 receptors causes release of IL-1beta-loaded microvesicles from human dendritic cells. *Blood* 2007;**109**(9):3856–3864.
- Baroni M, Pizzirani C, Pinotti M, et al. Stimulation of P2X7 receptors in human dendritic cells induces the release of tissue factor-bearing microparticles. *FASEB J* 2007;**21**(8):1926–1933.
- Vultaggio-Poma V, Falzoni S, Chiozzi P, et al. Extracellular ATP is increased by release of ATP-loaded microparticles triggered by nutrient deprivation. *Theranostics* 2022;**12**(2):859–874.
- Di Virgilio F, Sarti AC, Coutinho-Silva R. Purinergic signaling, DAMPs, and inflammation. *Am J Physiol Cell Physiol* 2020;**318**(5):C832–C835.
- Burnstock G. Purinergic signalling and neurological diseases: an update. *CNS Neurol Disord Drug Targets* 2017;**16**(3):257–265.
- Vultaggio-Poma V, Falzoni S, Salvi G, Giuliani AL, Di Virgilio F. Signalling by extracellular nucleotides in health and disease. *Biochim Biophys Acta Mol Cell Res* 2022;**1869**(5):119237.
- Lombardi M, Gabrielli M, Adinolfi E, Verderio C. Role of ATP in extracellular vesicle biogenesis and dynamics. *Front Pharmacol* 2021;**12**:654023.
- Ronquist KG, Ek B, Morrell J, et al. Prostatomes from four different species are able to produce extracellular adenosine triphosphate (ATP). *Biochim Biophys Acta* 2013;**1830**(10):4604–4610.

14. Boudreau LH, Ducheze AC, Cloutier N, et al. Platelets release mitochondria serving as substrate for bactericidal group IIA-secreted phospholipase A2 to promote inflammation. *Blood* 2014;**124**(14):2173–2183.
15. Wang X, Gerdes HH. Transfer of mitochondria via tunneling nanotubes rescues apoptotic PC12 cells. *Cell Death Differ* 2015;**22**(7):1181–1191.
16. Ducheze AC, Boudreau LH, Naika GS, et al. Platelet microparticles are internalized in neutrophils via the concerted activity of 12-lipoxygenase and secreted phospholipase A2-IIA. *Proc Natl Acad Sci USA* 2015;**112**(27):E3564–3573.
17. Hayakawa K, Esposito E, Wang X, et al. Transfer of mitochondria from astrocytes to neurons after stroke. *Nature* 2016;**535**(7613):551–555.
18. Gao L, Zhang Z, Lu J, Pei G. Mitochondria are dynamically transferring between human neural cells and alexander disease-associated GFAP mutations impair the astrocytic transfer. *Front Cell Neurosci* 2019;**13**:316.
19. Saha T, Dash C, Jayabalan R, et al. Intercellular nanotubes mediate mitochondrial trafficking between cancer and immune cells. *Nat Nanotechnol* 2022;**17**(1):98–106.
20. Pang Y, Zhang C, Gao J. Macrophages as emerging key players in mitochondrial transfers. *Front Cell Dev Biol* 2021;**9**:747377.
21. Fairley LH, Grimm A, Eckert A. Mitochondria transfer in brain injury and disease. *Cells* 2022;**11**(22):3603. <https://doi.org/10.3390/cells11223603>.
22. Scheiblich H, Dansokho C, Mercan D, et al. Microglia jointly degrade fibrillar alpha-synuclein cargo by distribution through tunneling nanotubes. *Cell* 2021;**184**(20):5089–5106.e21.
23. Sanz JM, Chiozzi P, Ferrari D, et al. Activation of microglia by amyloid {beta} requires P2X7 receptor expression. *J Immunol* 2009;**182**(7):4378–4385.
24. Lian H, Roy E, Zheng H. Protocol for primary microglial culture preparation. *Bio Protoc* 2016;**6**(21):e1989. <https://doi.org/10.21769/BioProtoc.1989>.
25. Adinolfi E, Callegari MG, Ferrari D, et al. Basal activation of the P2X7 ATP receptor elevates mitochondrial calcium and potential, increases cellular ATP levels, and promotes serum-independent growth. *Mol Biol Cell* 2005;**16**(7):3260–3272.
26. Reynolds ES. The use of lead citrate at high pH as an electron-opaque stain in electron microscopy. *J Cell Biol* 1963;**17**(1):208–212.
27. Gulinelli S, Salaro E, Vuerich M, et al. IL-18 associates to microvesicles shed from human macrophages by a LPS/TLR-4 independent mechanism in response to P2X receptor stimulation. *Eur J Immunol* 2012;**42**(12):3334–3345.
28. D'Arrigo G, Gabrielli M, Scaroni F, et al. Astrocytes-derived extracellular vesicles in motion at the neuron surface: involvement of the prion protein. *J Extracell Vesicles* 2021;**10**(9):e12114.
29. Murgia M, Hanau S, Pizzo P, Ripa M, Di VF. Oxidized ATP. An irreversible inhibitor of the macrophage purinergic P2Z receptor. *J Biol Chem* 1993;**268**(11):8199–8203. Published 1993/04/15.
30. Boyer JL, Harden TK. Irreversible activation of phospholipase C-coupled P2Y-purinergic receptors by 3'-O-(4-benzoyl)benzoyl adenosine 5'-triphosphate. *Mol Pharmacol* 1989;**36**(6):831–835. Published 1989/12/01.
31. Yanez-Mo M, Siljander PR, Andreu Z, et al. Biological properties of extracellular vesicles and their physiological functions. *J Extracell Vesicles* 2015;**4**:27066.
32. Sarti AC, Vultaggio-Poma V, Falzoni S, et al. Mitochondrial P2X7 receptor localization modulates energy metabolism enhancing physical performance. *Function* 2021;**2**(2):zqab005. <https://doi.org/10.1093/function/zqab005>.
33. Gomperts BD. Involvement of guanine nucleotide-binding protein in the gating of Ca<sup>2+</sup> by receptors. *Nature* 1983;**306**(5938):64–66.
34. Steinberg TH, Newman AS, Swanson JA, Silverstein SC. ATP<sub>4</sub>- permeabilizes the plasma membrane of mouse macrophages to fluorescent dyes. *J Biol Chem* 1987;**262**(18):8884–8888. Published 1987/06/25.
35. Falzoni S, Munerati M, Ferrari D, Spisani S, Moretti S, Di Virgilio F. The purinergic P2Z receptor of human macrophage cells. Characterization and possible physiological role. *J Clin Invest* 1995;**95**(3):1207–1216.
36. Baricordi OR, Melchiorri L, Adinolfi E, et al. Increased proliferation rate of lymphoid cells transfected with the P2X7 ATP receptor. *J Biol Chem* 1999;**274**(47):33206–33208.
37. Bianco F, Ceruti S, Colombo A, et al. A role for P2X7 in microglial proliferation. *J Neurochem* 2006;**99**(3):745–758.
38. Monif M, Reid CA, Powell KL, Smart ML, Williams DA. The P2X7 receptor drives microglial activation and proliferation: a trophic role for P2X7R pore. *J Neurosci* 2009;**29**(12):3781–3791.
39. Chiozzi P, Sanz JM, Ferrari D, et al. Spontaneous cell fusion in macrophage cultures expressing high levels of the P2Z/P2X7 receptor. *J Cell Biol* 1997;**138**(3):697–706.
40. Lemaire I, Falzoni S, Zhang B, Pellegatti P, Di Virgilio F. The P2X7 receptor and Pannexin-1 are both required for the promotion of multinucleated macrophages by the inflammatory cytokine GM-CSF. *J Immunol* 2011;**187**(7):3878–3887.
41. Liu D, Gao Y, Liu J, et al. Intercellular mitochondrial transfer as a means of tissue revitalization. *Signal Transduct Target Ther* 2021;**6**(1):65.
42. Lawrence G, Holley CL, Schroder K. Parkinson's disease: connecting mitochondria to inflammasomes. *Trends Immunol* 2022;**43**(11):877–885.
43. Joshi AU, Minhas PS, Liddel SA, et al. Fragmented mitochondria released from microglia trigger A1 astrocytic response and propagate inflammatory neurodegeneration. *Nat Neurosci* 2019;**22**(10):1635–1648.
44. Watson DC, Bayik D, Storevik S, et al. GAP43-dependent mitochondria transfer from astrocytes enhances glioblastoma tumorigenicity. *Nat Cancer* 2023;**4**(5):648–664.
45. Morrison TJ, Jackson MV, Cunningham EK, et al. Mesenchymal stromal cells modulate macrophages in clinically relevant lung injury models by extracellular vesicle mitochondrial transfer. *Am J Respir Crit Care Med* 2017;**196**(10):1275–1286.
46. Brestoff JR, Wilen CB, Moley JR, et al. Intercellular mitochondria transfer to macrophages regulates white adipose tissue homeostasis and is impaired in obesity. *Cell Metab* 2021;**33**(2):270–282.e8.
47. Giuliani AL, Sarti AC, Di VF. Extracellular nucleotides and nucleosides as signalling molecules. *Immunol Lett* 2019;**205**:16–24.
48. Di Virgilio F, Vultaggio-Poma V, Falzoni S, Giuliani AL. Extracellular ATP: a powerful inflammatory mediator in the central nervous system. *Neuropharmacology* 2023;**224**:109333.
49. Ferrari D, Villalba M, Chiozzi P, Falzoni S, Ricciardi-Castagnoli P, Di Virgilio F. Mouse microglial cells express a plasma membrane pore gated by extracellular ATP. *J Immunol* 1996;**156**(4):1531–1539. Published 1996/02/15.

50. Jackson MV, Morrison TJ, Doherty DF, et al. Mitochondrial transfer via tunneling nanotubes is an important mechanism by which mesenchymal stem cells enhance macrophage phagocytosis in the in vitro and in vivo models of ARDS. *Stem Cells* 2016;**34**(8):2210–2223.
51. Falzoni S, Chiozzi P, Ferrari D, Buell G, Di Virgilio F. P2X7 receptor and polykation formation. *Mol Biol Cell* 2000;**11**(9):3169–3176.
52. Gu BJ, Wiley JS. P2X7 as a scavenger receptor for innate phagocytosis in the brain. *Br J Pharmacol* 2018;**175**(22):4195–4208.
53. Chiozzi P, Sarti AC, Sanz JM, et al. Amyloid beta-dependent mitochondrial toxicity in mouse microglia requires P2X7 receptor expression and is prevented by nimodipine. *Sci Rep* 2019;**9**(1):6475.